# First experimental results on multi-angle DVB-S based passive ISAR exploiting multipolar data

Fabrizio Santi*, Iole Pisciottano+, Debora Pastina*, Diego Cristallini+

* Department of Information Engineering, Electronics and Telecommunications (DIET) – Sapienza University of Rome, Italy
fabrizio.santi@uniroma1.it, debora.pastina@uniroma1.it

+ Fraunhofer Institute for High Frequency Physics and Radar Techniques (FHR), 53343, Wachtberg, Germany
iole.pisciottano@fhr.fraunhofer.de, diego.cristallini@fhr.fraunhofer.de

***Abstract*—This work investigates the potentialities of a passive multidimensional ISAR imaging based on DVB-S transmitters of opportunity. Image fusion methods exploiting diversities in both the spatial and polarimetric domains are introduced, aiming at achieving an image with better quality than the images acquired by the individual observation angles and/or polarimetric channels. An analysis using experimental datasets comprising a passive receiver able to collect signals in both the horizontal and vertical polarizations, a cooperative turning ferry, and an Astra satellite has been provided.**

***Keywords—passive radar, passive ISAR, DVB-S based passive ISAR, passive polarimetry, multidimensional imaging***

## I. INTRODUCTION

One of the most recent developments in the field of passive radar is the possibility to produce images of the detected targets by means of inverse synthetic aperture radar (ISAR) processing. Passive ISAR is a powerful tool for the characterization of the scattering properties of radar targets using systems with no requirements for dedicated transmitting segments. Over the last years, most of the research efforts in the passive ISAR field concerned the exploitation of terrestrial illuminators of opportunity, such as FM [1], DVB-T [2] and, for short-range/indoor applications, Wi-Fi signals [3].

An alternative to terrestrial-based passive radar is represented by the exploitation of satellite transmitters of opportunity, such as navigation or communication satellites. With respect to their terrestrial counterparts, satellites can provide a wider accessibility on the global scale, enabling radar operations even in remote areas. Moreover, they are less susceptible to multipath effects and are less vulnerable in case of natural or man-made disasters. With specific regard to passive ISAR, global navigation satellite systems (GNSS) and digital video broadcasting-satellite (DVB-S) have been very recently considered for ship target imaging [4]-[8].

DVB-S satellites represent indeed an interesting choice for passive maritime targets imaging. Because they operate in geostationary orbits, a permanent coverage over continental areas, even off-shore, is assured. Moreover, a single satellite carries multiple transponders, each broadcasting signals over a bandwidth of tens of MHz, being 32 MHz the value that occurs the most. For such a value, a range resolution up to 6.5 meters could be achieved (for small bistatic angles), which could be even enhanced combining multiple transponders operating on close operative bands [9]. Furthermore, DVB-S works in the Ku-band with carrier frequencies in the range 10.7 GHz – 12.75 GHz, thus assuring a high sensibility in Doppler, potentially providing a high cross-range resolution.

Despite the potentially high geometrical resolution of the DVB-S based passive ISAR products, the transmitted waveforms are not intended for radar purposes, posing a number of limitations. The main challenge for satellite-based passive radar systems is the low power density of received signals over the Earth‘s surface, which limits the signal-to-noise ratio (SNR) of the resulting images, and therefore the amount of information that can be extracted. A common solution to increase the SNR is extending the coherent processing interval (CPI). Nevertheless, the de-correlation of the e. m. response of the target imposes an upper bound to the maximum CPI extent, which can be quite short (typically about 1 s) for a ~3 cm wavelength such as those of DVB-S signals.

To overcome the limitations imposed by the low power budget and to increase the target information space, solutions based on multidimensional configurations can be considered [10], [11]. For example, in [4], a method for fusing GNSS-based passive ISAR images achieved over consecutive time instants (frames) has been proposed. Other than the temporal diversity, spatial diversity can be exploited. Multi-angle images achieved using spatially distributed transmitters [5] or multiple looks at the receiver segment [8] can be combined: depending on the particular viewing angles, different scattering centers could be observed and therefore a higher capability to recognize the target shape can be obtained.

Leveraging data acquired over different polarization states is a further strategy to expand the dimensionality of the imaging system. Scattering mechanisms are sensitive to the polarization states of the e. m. radiation, thus allowing for a much richer information set to be garnered from which target classification can be improved. DVB-S transponders are overlapped and interleaved in the horizontal (H) and vertical (V) polarizations, therefore multipolar passive ISAR imaging is fundamentally possible [12].

In this work, we consider the formation of DVB-S based passive ISAR images of ship targets by exploiting spatial and polarimetric diversities. In particular, we focus on the combination of the individual images acquired over multiple look angles and different polarimetric channels. Methods to combine the individual images into a unique multidimensional image have been introduced, with the ultimate goal to achieve a greater capability to extract geometrical features of the imaged target. An experimental analysis has been then conducted to assess the effectiveness of the approaches. A ferry equipped with an inertial measurement unit (IMU) has been employed as cooperative target; for it was yawing, it gave us the chance to process data frames under a multitude of receiver observation angles. Signals emitted by an Astra satellite in both the H and V polarizations have been acquired by the passive receiver SABBIA developed at Fraunhofer FHR.

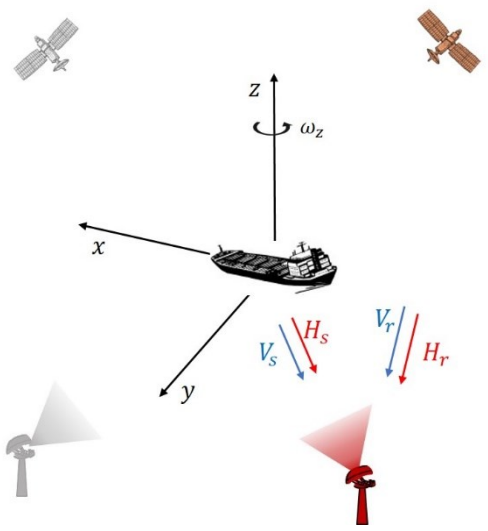


Fig. 1. System geometry.

The remainder of this paper is as follows. Section II details the polarimetric passive ISAR processing, while Section III introduces the multi-angle imaging with multipolar data; experimental analysis is provided in Section IV and Section V closes the paper.

## II. DVB-S Based Passive ISAR

### A. System overview

The operative conditions of the system are sketched in Fig. 1 in a target fixed $(x, y, z)$ reference system. A DVB-S satellite emits signals simultaneously in both polarizations that are captured by the reference antenna of a passive receiver. Also, the signals are reflected by a target and collected by the surveillance antenna of the receiver. Both the reference and surveillance acquisition chains employ two separated channels for collecting the H/V polarized signals.

It must be pointed out that the challenging passive environment makes necessary some adaptations to enable polarimetric operations in the framework under consideration. While in conventional radar polarimetry H and V polarized signals are alternatively transmitted and simultaneously received, DVB-S transponders broadcast signals simultaneously in the two polarizations, [13]: in our case, polarimetric operations are implemented by cross-correlating orthogonally polarized signals at the reference and surveillance channel. It must be stressed that reference and surveillance antennas are differently oriented. Therefore, two couples of orthogonal planes must be defined: hereinafter, $H_r$ and $V_r$ denote the H/V signals states at the reference channels, while $H_s$ and $V_s$ refer to the surveillance channel.

In line with the experimental scenario described in Section IV, we assume the target is rotating according to a yaw rate $\omega_z$. Therefore, images taken at a variety of target attitudes [i.e., different transmitter and receiver positions in the $(x, y, z)$ space] over time can be focused. Thanks to the availability of multipolar data, for each image time up to four images can be focused: two co-polarized, $H_rH_s$ and $V_rV_s$, and two cross-polarized, $H_rV_s$ and $V_rH_s$. Hereafter, the letter $\gamma$ will denote the particular polarimetric output, namely $\gamma = \{H_rH_s, V_rV_s, H_rV_s, V_rH_s\}$. It is worth to point out that the inherent bistatic nature of the passive systems makes the cross-polarized terms different, namely $I_{H_rV_s} \neq I_{V_rH_s}$.

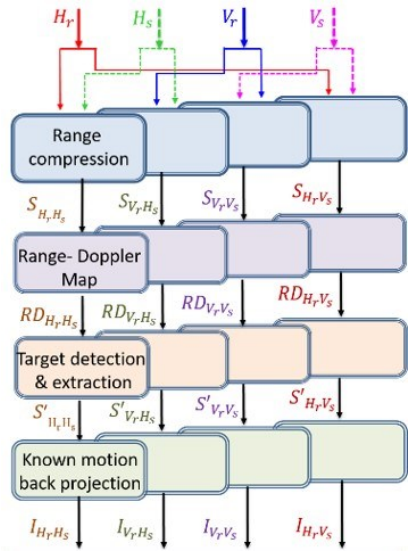


Fig. 2. Single channel ISAR processing scheme.

### B. Single-channel data processing

For the generic polarimetric combination $\gamma$ mentioned above, the same single processing has been applied to obtain the corresponding passive ISAR image, as described below. Fig. 2 depicts the block diagram of the processing.

Firstly, the continuous wave DVB-S signals are partitioned in consecutive batches with constant duration $T_{int}$ in order to define equivalent (fast-time $\tau$, slow-time $t_n$) domains. The range compression is obtained for each batch by cross-correlating the complex envelope of the signal received in the surveillance channel $\chi(\tau,t_n)$ (being $\chi = \{H_s, V_s\}$) with the reference signal $\xi(\tau,t_n)$ (being $\xi = \{H_r, V_r\}$) leading to the cross-ambiguity function (CAF). Consecutive batches are then Fourier transformed in the Doppler domain:

$$S_\gamma(\tau, f_D) = \sum_{n=0}^{N-1} \xi(nT_s) \cdot \chi^*(nT_s - \tau)\, e^{-j2\pi f_D T_s/N} \qquad (1)$$

where $f_D$ is the bistatic Doppler, $Ts = f_s/N$ being $f$ the sampling frequency and $N$ is obtained by the product of the Doppler bins number $N_d$ and the range bins number $N_r$.

Then, the target of interest can be detected and the region of the Range-Doppler (RD) map containing it can be cropped for the following ISAR processing [14]. If necessary, the ISAR aperture time (i.e., the CPI) can be extended by juxtaposing data corresponding to consecutive RD maps.

Each dataset is then processed exploiting a priori information regarding the target motion. The known motion back projection (KM-BP) algorithm introduced in [6] has been in this case applied to each polarization pair as follows

$$I_\gamma(x, y) = \sum_n S'_\gamma(f, t_n)\, e^{j2\pi f \frac{r_b(x,y,t_n)}{c}} \qquad (2)$$

where $(x, y)$ is a grid of points defined in the target fixed coordinate system ($z=0$ in this analysis), $S'_\gamma(f, t_n)$ is the range compressed signal in (fast frequency $f$, slow-time $t_n$) domain after the target extraction at the slow time instant $t_n \in$ CPI. $r_b$ is the bistatic range retrieved from the IMU mounted on the target by considering the relative distances between the target and transmitter (namely $d_{T_xT_g}$) and between target and

receiver (namely $d_{R_xT_g}$), and corrected for the baseline from transmitter to receiver (namely $d_{T_xR_x}$):

$$r_b(x,y,t_n) = d_{T_xT_g}(x,y,t_n) + d_{R_xT_g}(x,y,t_n) - d_{T_xR_x}(t_n) \quad (3)$$

Finally, let us assume that multipolar acquisitions are available on M different target aspect angles, for instance while the target is yawing, see following Section IV. To explicit this dependency, the passive ISAR image of (2) can be re-written as $I_\gamma(x,y,m)$, with $m = \{1,\dots,M\}$.

## III. Multi-angle and Multipolar ISAR Imagery

As well known, target reflectivity varies with the state of the e.m. radiation. Polarimetric decomposition methods are usually applied to recognize the scattering processes produced by the observed object, providing meaningful information for classification procedures [17]. In [12], a first investigation on the capability of DVB-S based passive polarimetric ISAR to separate the scattering mechanisms has been provided, showing that different target structures behave differently in the polarimetric domain.

A different approach to exploit multipolar data is operating directly in the image domain. Such class of methods gives up to discriminate the scattering processes, but rather they aim at combining the multipolar images on a pixel basis to achieve a new image of better quality. The underlying idea of such methods is that the different sensitivity of a target scatterer to a particular combination of transmitted/received polarized signal can make it more or less visible in the different polarimetric images. Therefore, a proper combination of the images can provide a more comprehensive representation of the full target structure.

At the same time, the variation of the relative target-to-receiver line-of-sight (LOS) during the observation time makes possible to process radar returns observed from different perspectives. The variation of the target signature over the different viewing angles represents a further source of diversity. Particularly, different structures of the target will be directly facing the surveillance antenna, so that concentration of brighter returns in different parts of the imaged targets can be expected. Furthermore, the shape of the point spread function of the image will vary with the particular bistatic geometry, so that individual scatterers that cannot be resolved in a particular image can be distinguished when observed under a different angle [8]. In the following, we will detail few approaches to fruitfully combine the multi-angle and multipolar ISAR images to achieve enhanced ISAR products, where an improved capability to extract the target size/shape can be obtained.

A straightforward approach to fuse the images is performing a Quadratic Integration (QI). The $I_{QI}(x,y)$ multi-angle-multipolar image can be obtained as

$$I_{QI}(x,y) = \sum_{m=1}^{M}\sum_{\gamma} I_\gamma(x,y,m) \quad (4)$$

This approach aims at exploiting the low correlation level of the background which is expected among the images acquired under the different observation angles and polarimetric channels. Fluctuations of the disturbance contribution can be therefore reduced, while target scatterers can be integrated thus potentially reaching an image with increased SNR. Nevertheless, as the position of the dominant scattering centers is expected to vary among the combined images, this criterion could suffer for significant information loss.

Taking into account the expected variation of the dominant parts observed in the different images, a combined image following a maximum (MAX) operator could be considered. The $I_{MAX}(x,y)$ image is achieved as

$$I_{MAX}(x,y) = \max_m \left\{ \max_\gamma I_\gamma(x,y,m) \right\} \quad (5)$$

This particular combination rule aims at keeping in the final image all the brightest scattering points observed. This is a nice property in the cases of strong de-correlation of the target returns among all the channels. However, two main of problems can be predicted. First, the noise background degrades, as the fluctuations cannot be broken down; moreover, scatterers intensities cannot fully benefit of being observed in the different channels.

The limitations of the QI and MAX operators arise from the fact that they combine the images regardless the specific content of the pixels. A different strategy is resorting to an adaptive approach relying on a measure of the significance level of a pixel. This approach has been proposed in [5]: for each pixel position, the local level of SNR is evaluated and then used to weigh the pixel contribution in the final image. This combination strategy has been here considered to combine the multipolar images pertaining the particular observation angle. Specifically, the Weighted Quadratic Integration (WQI) multipolar image for the $m$th angle is achieved as

$$I_{WQI_m}(x,y) = \sum_{\gamma} w_\gamma(x,y,m) \times I_\gamma(x,y,m) \quad (6)$$

where $w_\gamma(x,y,m) = \frac{SNR\{I_\gamma(x,y,m)\}}{SNR\{I_\gamma(x,y,m)\}+1}$ is the local weight based on the SNR evaluated in the $m$th angle and $\gamma$th polarimetric channel. A multi-angle-multipolar image $I_{WQI}(x,y)$ can be then obtained by using the same criterion, namely

$$I_{WQI}(x,y) = \sum_{m=1}^{M} w_m(x,y) \times I_{WQI_m}(x,y) \quad (7)$$

where $w_m(x,y) = \frac{SNR\{I_{WQI_m}(x,y)\}}{SNR\{I_{WQI_m}(x,y)\}+1}$.

This combination strategy aims at adaptively integrating the contributions of one particular scatterer over the multiple channels. Even though, under the individual observation angle, a scatterer provided a bright return only in a single polarimetric channel, the weighted summation (6) ensures a higher probability to contribute to the $I_{WQI_m}$ image than that achievable with the unweighted summation. Moreover, unlike the MAX operator, if the scatterer gives rise to significant contributions in multiple polarimetric channels, the visibility of that scatterer in the combined image will rise accordingly. Furthermore, pixels with a low mean intensity over the channels will likely belong to the disturbance background: therefore, they will be averaged thus reducing the disturbance fluctuations. Similar considerations apply when performing (7) to combine the M $I_{WQI_m}$ images into the multi-angle-multipolar image.

(a)


(b)

Fig. 3 Receiving system (a) and cooperative target (b).

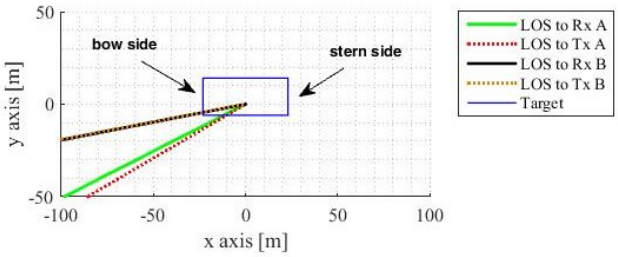


Fig. 4 Transmitter and receiver line-of-sights (top-view).

## IV. Experimental Results

Experimental trials have been carried out on the Rhine river near Bonn, Germany. The receiving hardware is the passive radar system SABBIA, developed at the Fraunhofer FHR [see Fig. 3(a)]. The system was installed on the bank of the river acquiring direct and reflected signals emitted by a DVB-S satellite in both the H/V polarizations. More details about the SABBIA system can be found in [15]. As illuminator of opportunity, we have considered the geostationary satellite ASTRA 1KR located at the 19.2° East orbital position [16], emitting signals in both polarizations within the Ku-band. During the acquisitions, the signals have been collected with an instantaneous signal bandwidth of 80 MHz centered on 11347 MHz.

During the experimental trials, a cooperative ferry was available [see Fig. 3(b)]. The ferry was equipped with an IMU to record both its position and its attitude. During the acquisitions, the ferry was rotating with a quite stable yaw motion. Therefore, images corresponding to multiple receiver positions in the target-fixed reference system (see Fig. 1) were available. Table I lists the acquisition parameters corresponding to two different frames and Fig. 4 shows the top-view of the transmitter and receiver LOSs. As it is apparent, different parts of the ferry directly face the receiving antenna, so that a variation of the target signature is expected. This variation will be exploited along with the polarimetric diversity to enhance the quality of the image products.

TABLE I. Acquisition parameters

| Frame | CPI | Receiver observation angle* | Yaw rate $\omega_z$ |
|---|---|---|---|
| A | 0.8 s | 243° | 2.0 °/s |
| B | 0.8 s | 260° | 2.4 °/s |

* measured clockwise from y axis

The target motion information provided by the IMU is exploited to form ISAR images in the target-fixed reference system via KM-BP (see Section II.B). The resulting single polarimetric channel images for data frames A and B are shown in Fig. 5 and Fig. 6, respectively, where the 0 dB level denotes the mean background level. The white dotted rectangle sketches a simplified target model highlighting the four sides of the ferry. The IMU is obviously located in the origin position (0,0).

In both the considered data frames, a significant variation of the images can be observed among the different polarimetric channels. For example, the co-polar image $I_{H_rH_s}$ for the geometry A [Fig. 5 (a)] shows a strong return in the central part of the ferry, corresponding the superstructure where the IMU is located [see Fig. 3 (b)]. In contrast, the cross-polar image $I_{V_rH_s}$ [Fig. 5 (c)] shows less strong returns in that area, whereas brightest scattering points can be observed in the left and right areas corresponding to the deck. It is also worth to point out that the cross-polar images $I_{V_rH_s}$ and $I_{H_rV_s}$, although similar, are actually different, because of the bistatic geometry of the acquisition.

The different behavior of the different parts of the target structure among the polarimetric channels is confirmed also looking at images pertaining the data frame B. In this case, a lower level of SNR than in frame A can be observed. However, it is possible to appreciate the different dominant scattering centers arising because the different combination of signal states at the reference/surveillance channel. For example, the 'bow' side is well visible in the co-polar images $I_{H_rH_s}$ and $I_{V_rV_s}$, whereas is the 'stern' area giving rise to dominant contributions in the cross-polar images $I_{H_rV_s}$ and $I_{V_rH_s}$.

For each observation angle, the multipolar images have been obtained by the combination rules (4), (5) (setting m = A or m = B), and (6). Fig. 7 shows the QI, MAX, and WQI images pertaining the frame B, where a better quality of these multipolar images than the single channel products in Fig. 6 can be observed. Despite the low SNR level observed with this frame, relevant characteristics of the target structure are more pronounced in the multipolar products. Bright spots are well visible in both the bow and stern sides; significant contributions in the central part, which could be observed with difficulty in the individual images, can be now quite clearly recognized. The fluctuations of the background are clearly reduced, allowing for a higher capability of extraction of the target segment. Similar considerations apply for the multipolar images pertaining data frame A (images are not shown in the paper for length constraints), where the higher SNR allows to recognize more patches of the ferry structure.

Comparing the images in Fig. 5 and Fig. 6, the different target signature under the different observation angles is evident. For data frame A, the frontal part of the ferry is more evident than in data frame B. Indeed, this side of the ferry is

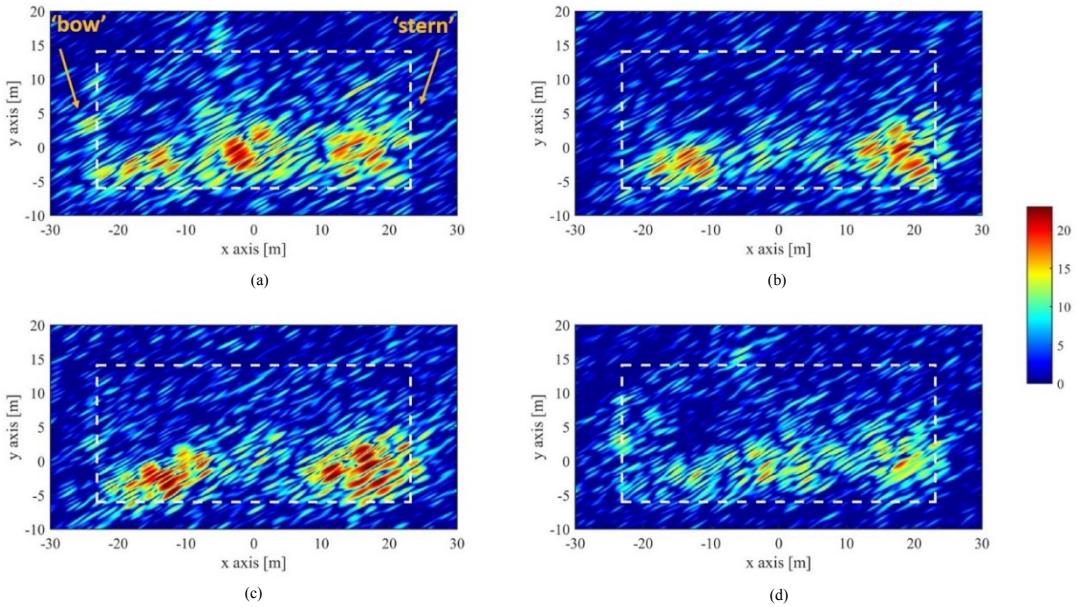


Fig. 5 Single channel images viewing angle A – (a) $I_{HrHs}$, (b) $I_{HrVs}$, (c) $I_{VrHs}$, (d) $I_{VrVs}$.

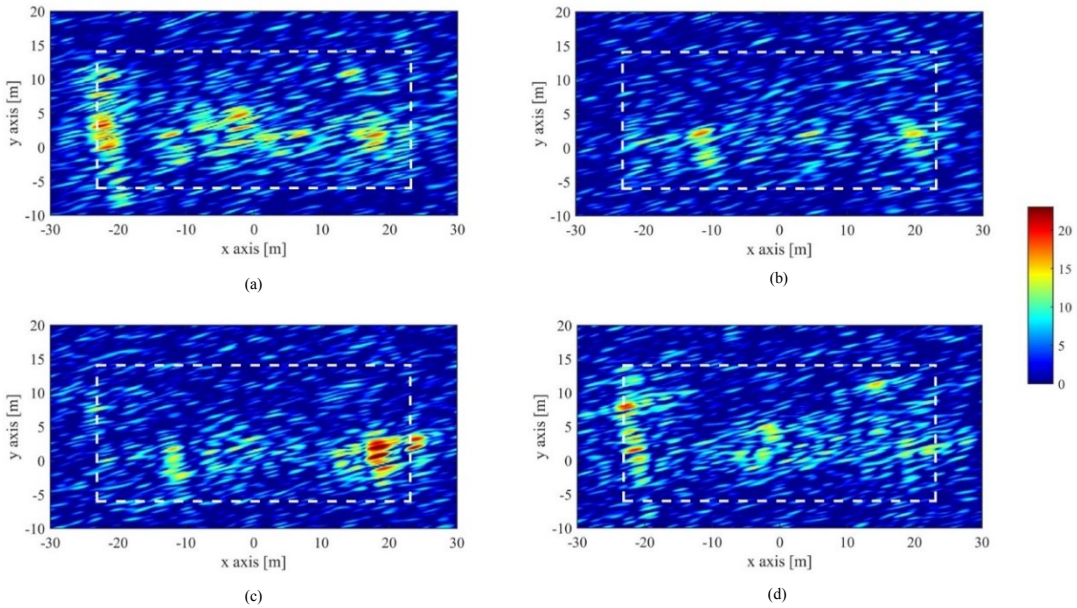


Fig. 6 Single channel images viewing angle B – (a) $I_{HrHs}$, (b) $I_{HrVs}$, (c) $I_{VrHs}$, (d) $I_{VrVs}$.

in full visibility of the receiving antenna during frame A, while it is partly shadowed during frame B (see Fig. 4). Whereas, in data frame B, the bow side, directly facing the receiver, gives rise to a cluster of bright spots nicely aligning over that segment of the ferry shape. Enhanced capability to recognize the ferry structure are expected by combining the multipolar images over the different viewing angles.

Fig. 8 shows the multi-angle-multipolar images achieved via (4), (5), and (7). A higher capability to recognize (and therefore extract) the geometrical shape has been obtained, as the bright regions of the images nicely fit into the rectangular area defining the ferry area. The bow, the central superstructure and the deck areas surrounding it are all well visible, condition that was not obtained in the individual angle/polarimetric channels. The fluctuations background has been simultaneously reduced, ensuring an improved capability in extracting the pixels actually belonging to the target.

Even though the images achieved with the different fusion strategies are quite similar, some differences can be appreciated. Table II lists the values of the image contrast (IC) of the single-angle multipolar and multi-angle-multipolar images (please note that such values must be compared in parity of combined images, namely the IC values must be compared inside the individual row). It can be observed that in all the analyzed cases the MAX and WQI operators provided higher IC values than the QI. The QI is well performing against the background (assuming a complete decorrelation of the disturbance among all the channels), but the strong variation of the target response over the channels implies integration losses. MAX and WQI provide higher integration gain for the pixels likely belonging to the target, so that higher SNR values can be appreciated in Fig. 7 (c) a Fig. 8 (c). The IC values for these operators are also very close, with the MAX that seems slightly outperform the WQI. However, the background behavior is expected to get worse

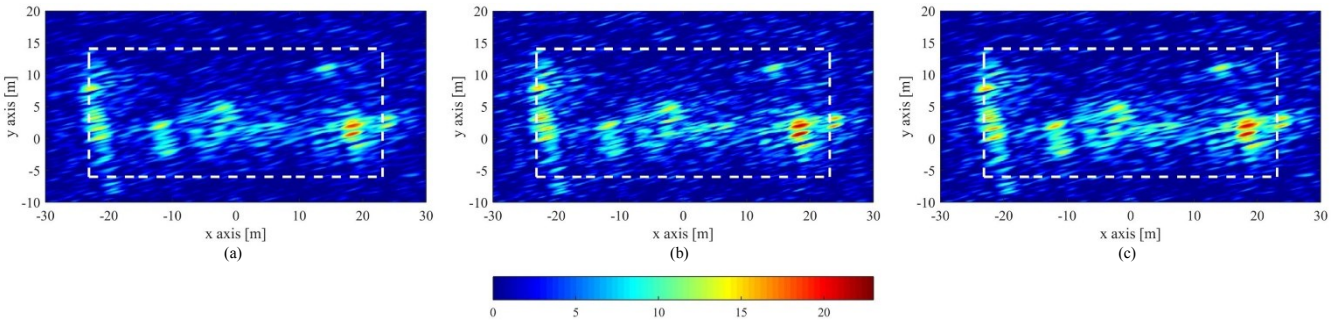


Fig. 7 Single angle – multipolar images, viewing angle B – (a) Quadratic Integration, (b) Max, (c) Weighted Quadratic Integration.

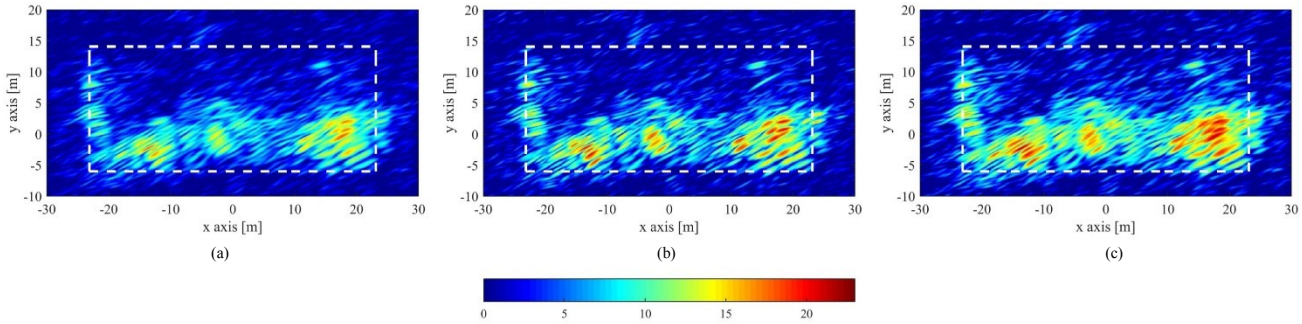


Fig. 8 Multi–angle–multipolar images – (a) Quadratic Integration $I_{QI}$, (b) Max $I_{MAX}$, (c) Weighted Quadratic Integration $I_{WQI}$.

TABLE II. IMAGE CONTRASTS

| | QI | MAX | WQI |
|---|---|---|---|
| Angle A - multipolar | 1.98 | 2.19 | 2.24 |
| Angle B - multipolar | 1.57 | 2.04 | 1.94 |
| Multi-angle - multipolar | 1.50 | 1.98 | 1.94 |

with a non-linear combination rule as the MAX. Further analysis will be conducted in the future to separate the target segment from the background to provide an automated estimation of the target size.

## V. CONCLUSIONS

In this work, we addressed a passive multidimensional ISAR imaging using DVB-S illuminators of opportunity. Diversity in both the angular and polarimetric domains have been exploited to achieve ISAR products with improved capability of extraction/reconstruction of the target segment/shape in the fused images.

Experimental results achieved under controlled conditions proved that a significant enhancement of the imaging capability of man-made targets can be obtained by properly fusing the information from the different illumination angles and polarimetric channels, thus partially overcoming the severe limitations imposed by the exploitation of satellite signals of opportunity.

## REFERENCES

[1] F. Colone, D. Pastina, V. Marongiu, "VHF cross-range profiling of aerial targets via passive ISAR: signal processing schemes and experimental results," *IEEE Trans. Aero. Elect. Syst*., vol. 53, no. 1, pp. 218-235, Feb. 2017.

[2] D. Olivadese, E. Giusti, D. Petri, *et al*., "Passive ISAR with DVB-T signals," *IEEE Trans. Geosci. Remote Sens*., vol. 51, no. 8, pp. 4508-4517, Aug. 2013.

[3] D. Pastina, F. Colone, T. Martelli, P. Falcone, "Parasitic exploitation of Wi-Fi signals for indoor radar surveillance," *IEEE Trans. Veh. Tech*., vol. 64, no. 4, pp. 1401-1415, Apr. 2015.

[4] D. Pastina, F. Santi, F. Pierlaice, M. Antoniou, M. Cherniakov, "Passive radar imaging of ship targets with GNSS signals of opportunity," *IEEE Trans. Geosci. Remote Sens*., in press.

[5] F. Santi, D. Pastina, M. Antoniou, M. Chenriakov, "GNSS-based multistatic passive radar imaging of ship targets," *IEEE RadarConf*, Washingthon, DC, USA, Apr. 2020, pp. 601-606.

[6] I. Pisciottano, D. Cristallini, D. Pastina, "Maritime target imaging via simultaneous DVB-T and DVB-S passive ISAR," *IET Radar Sonar Nav.*, vol. 13, no .9, pp. 1479-1487, Sep. 2019.

[7] T. V. Cao, R. Merlino, H. –T. Tran, "Using passive ISAR for imaging maritime targets," *Int. Radar Sym*., Bonn, Germany, Jun. 2018.

[8] F. Santi, I. Pisciottano, D. Cristallini, D. Pastina, "Preliminary investigation toward multi-frame DVB-S based passive ISAR," *13th EUSAR Conf.,* 29 Mar.-1 Apr. 2021.

[9] S. Brisken, M. Moscadelli, V. Seidel, C. Schwark, "Passive radar imaging using DVB-S2," *IEEE RadarConf*, Seattle, WA, Apr. 2017, pp. 0552-0556.

[10] M. Martorella (Ed.), *Multidimensional Radar Imaging*, SciTech Pub., Six Hills Way, Stevenage, UK, 2019.

[11] S. Brisken, D. Matthes, T. Mathy, and J. G. Worms, "Spatially diverse ISAR imaging for classification performance enhancement," *Int. J. Elec. Telecom.*, vol. 57, no. 1, pp. 15 –21, 2011.

[12] I. Pisciottano, F. Santi, D. Pastina, D. Cristallini, "DVB-S Based Passive Polarimetric ISAR—Methods and Experimental Validation," *IEEE Sensors Journal*, vol. 21, no. 5, pp. 6056-6070, Mar. 2021.

[13] http://frequencyplansatellites.altervista.org/Astra/Astra_1KR.pdf, URL accessed on 2020-10-26.

[14] J. L. Garry, G. E. Smith, "Passive ISAR part I: framework and considerations", *IET Radar Sonar Nav.*, vol. 13, no. 2, pp. 169-180, Feb. 2019.

[15] I. Pisciottano, D. Cristallini, J. Schell, V. Seidel, "Passive ISAR for Maritime Target Imaging: Experimental Results", *Int. Radar Symp.*, Bonn, Germany, Jun. 2018.

[16] ASTRA 1KR's mission, [Online]. Available: https://www.ses.com/our-coverage#/explore/satellite/335.

[17] R. Paladini, M. Martorella, F. Berizzi, "Classification of Man-Made Targets via Invariant Coherency-Matrix Eigenvector Decomposition of Polarimetric SAR/ISAR Images," *IEEE Trans. Geosci. Remote Sens*., vol. 49, no. 8, pp. 3022-3034, Aug. 2011.